Transient Analysis of Lossy Transmission Lines: an Efficient Approach Based on the Method of Characteristics

Transient Analysis of Lossy Transmission Lines: an Effective Approach Based on the Method of Characteristics

S. Grivet-Talocia[‡], H-M. Huang[⋆], A. E. Ruehli[†], F. Canavero[‡], I. M. Elfadel[†]

[‡] Dept. of Electronics, Politecnico di Torino, C. Duca degli Abruzzi 24, 10129 Torino, Italy

Tel: +39-011-564-4104, Fax: +39-011-564-4099, E-mail: {grivet,canavero}@polito.it

[⋆] IBM Microelectronics Division, Route 52, Hopewell Junction, NY 12533

Tel: (845) 892-2723, Fax: (845) 892-2066, E-mail: haohuang@us.ibm.com

[†] IBM T. J. Watson Research Center, P.O. Box 218, Yorktown Heights, NY 10598

Tel: (914) 945-1592, E-mail: {ruehli,elfadel}@us.ibm.com

Revised manuscript: November 5, 2003

Abstract: *This paper is devoted to transient analysis of lossy transmission lines characterized by frequency-dependent parameters. A public dataset of parameters for three line examples (a module, a board, and a cable) is used, and a new example of on-chip interconnect is introduced. This dataset provides a well established and realistic benchmark for accuracy and timing analysis of interconnect analysis tools. Particular attention is devoted to the intrinsic consistency and causality of these parameters. Several implementations based on generalizations of the well-known Method-of-Characteristics are presented. The key feature of such technique is the extraction of the line modal delays. Therefore, the method is highly optimized for long interconnects characterized by significant propagation delay. Nonetheless, the method is also successfully applied here to a short high/loss on-chip line, for which other approaches based on lumped matrix rational approximations can*

also be used with high efficiency. This paper shows that the efficiency of delay extraction techniques is strongly dependent on the particular circuit implementation, and several practical issues including generation of rational approximations and time step control are discussed in detail.

Keywords: *Lossy Transmission Lines, Transient Analysis, Causality, Hilbert transform, Method of Characteristics*

1 Introduction

Electrical interconnects at chip, multichip, package, and board level constitute one of the most critical parts for the signal integrity of all electronic systems. Nonetheless, an accurate and efficient transient simulation of electrical interconnects is still a challenging task even in the most advanced circuit solvers. This is due to the intrinsic difficulties in the design of stable algorithms for the time-domain analysis of structures with frequency-dependent parameters. Indeed, it is well known that accurate interconnect models must take into account metal (skin effect) and dielectric losses, which lead to possibly large attenuation at increasing frequency. The underlying physics is best captured using a frequency-domain approach, leading to constitutive parameters with a complex dependence on frequency. A robust approximation is therefore required for the conversion to time domain of the constitutive line equations and the subsequent generation of a line macromodel to be employed in a transient simulation.

In this paper we investigate several implementations of line macromodels derived from the general approach of the well-known Method of Characteristics (MoC), which was first used for transmission lines by Branin [1]. The MoC model is based on the extraction of the line propagation delay and is exact if applied to lossless transmissions lines. To include losses, the MoC model has evolved over the years to keep in steps with the advances in the hardware technologies. Numerous improvements have been made such that the approach can be applied to multiple lossy transmission lines. This has been accomplished by augmenting the model such that the admittances and the sources representing the delay could model the lossy transmission line behavior (see, e.g., [11, 18, 19]). A brief description of the MoC based approach is detailed in Section 3. The aspects that are

critical for the practical implementation are detailed and several choices are discussed here in some detail. The key steps are extraction of the line delays, rational fitting of suitable delayless transfer functions, and generation of a macromodel to be embedded in some SPICE-like circuit solver. As a result, several different algorithms have been coded and embedded in a single circuit simulation environment, the Linux version of IBM's PowerSPICE program. This allows to draw meaningful comparisons in terms of accuracy and execution time.

The different modeling strategies developed during this work are applied to four benchmark lines, namely an on-chip line, MultiChip Module (MCM) line, a long cable, and a Printed Circuit Board (PCB) line. The last three examples were first discussed in [21], where frequency tables of per-unit-length parameters are available. A new set of parameters is introduced here for an on-chip interconnect. The structures are briefly outlined in Appendix A. We remark that the specification of the frequency-dependent line parameters is a very critical point, since these parameters are related to each other by consistency relations based on the causality principle. Therefore, we have developed a consistency check procedure based on a discretization of the Hilbert transform that allows to verify apriori whether the line model is self-consistent. This procedure is outlined in Section 2. Finally, the transient numerical results are the subject of Section 4.

Let us first set the notations to be used throughout this paper. We consider a lossy multiconductor transmission line governed by the telegraphers equations, here stated in the Laplace domain

$$\begin{aligned} -\frac{d}{dz}\mathbf{V}(z,s) &= \mathbf{Z}(s)\ \mathbf{I}(z,s), \\ -\frac{d}{dz}\mathbf{I}(z,s) &= \mathbf{Y}(s)\,\mathbf{V}(z,s), \end{aligned} \tag{1}$$

where z represents the longitudinal coordinate along which signals propagate according to the quasi-TEM mode. The length of the line will be denoted as $\mathcal{L}$. The transmission line per-unit-length matrices $\mathbf{Y}(s)$ and $\mathbf{Z}(s)$ are defined as

$$\mathbf{Y}(s) = \mathbf{G}(s) + s\mathbf{C}(s) \quad \text{and} \quad \mathbf{Z}(s) = \mathbf{R}(s) + s\mathbf{L}(s) \tag{2}$$

with $\mathbf{G}(s)$, $\mathbf{C}(s)$, $\mathbf{R}(s)$ and $\mathbf{L}(s)$ denoting the per-unit-length conductance, capacitance, resistance, and inductance matrices, respectively. These four matrices are collectively indicated as frequency-dependent, per-unit-length (f-PUL) parameters. These parameters are usually specified at fixed frequency points $\{s_k = j\omega_k =$

$j2\pi f_k\}$ by means of transverse 2D electromagnetic simulation or measurement. This is also the case for the benchmark lines that will be analyzed throughout this paper.

2 Causality and Consistency of Line Parameters

One very important aspect which is often neglected in the analysis of frequency-dependent transmission lines is the internal consistency of the line model being adopted. In particular, the four f-PUL matrices $\mathbf{G}(s)$, $\mathbf{C}(s)$, $\mathbf{R}(s)$ and $\mathbf{L}(s)$ are not independent, being related by fundamental causality conditions. More precisely, the real and imaginary parts of both transverse admittance $\mathbf{Y}(s)$ and impedance $\mathbf{Z}(s)$ in (2) must be related by Hilbert transform according to the well-known Kramers-Krönig conditions [16, 20]. This implies that specification of frequency values for the four f-PUL matrices must take into account such conditions in order to insure a self-consistent line model. As an example, Figure 1 illustrates the typical effects induced on the transient responses by some causality violation in the line parameters. It is clear that any attempt to process flawed data which do not satisfy these conditions will possibly lead to spurious results. This section describes a procedure allowing for verification of causality conditions for tabulated f-PUL parameters.

We consider for illustration a generic matrix transfer function $\mathbf{K}(s)$ that we split into real and imaginary part

$$\mathbf{K}(s = j\omega) = \mathbf{A}(\omega) + j\mathbf{B}(\omega).$$

Several equivalent formulations of the causality relations can be applied. Here we follow [12]. The real-to-imaginary part consistency for the (pq) element is guaranteed by the following relation

$$B_{pq}(\omega) = \frac{1}{\pi}\int_0^\infty \frac{dA_{pq}(\omega')}{d\omega'} \ln\frac{|\omega' + \omega|}{|\omega' - \omega|} d\omega' \tag{3}$$

The practical implementation of (3) for the mapping $A_{pq}(\omega)$ to $B_{pq}(\omega)$ can be obtained via discretization. First, we replace the integral with a summation over small frequency intervals and we approximate the derivative with a piecewise constant expression over each interval. The remaining integral can be evaluated analytically. If we denote with $\mathbf{a}_{pq}$ and $\mathbf{b}_{pq}$ the vectors collecting the N discrete values of real and imaginary parts of the selected

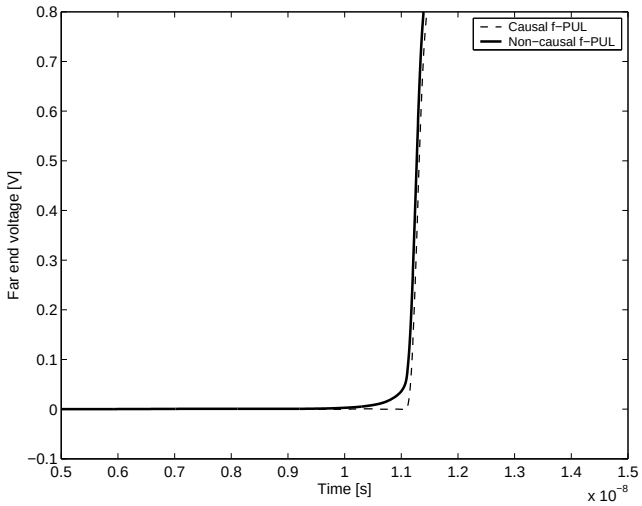

Figure 1: Transient solution of a ceramic MCM line illustrating the effects of non-consistent f-PUL parameters. The non-causal parameters were derived from a proper causal set by neglecting the frequency variation of the line inductance. The structure is a two-conductor coupled line. One of the two conductors is excited by a 100ps voltage step, the plot reports the transmitted voltage on the other end of the active conductor.

matrix entry at the prescribed frequency points, we get

$$\mathbf{b}_{pq} = \mathbf{H}\,\mathbf{a}_{pq} \tag{4}$$

where the $N \times N$ matrix $\mathbf{H}$ results from the discretization

$$B_{pq}(\omega_m) = \frac{1}{\pi}\sum_{k=1}^{N} \left.\frac{dA_{pq}(\omega')}{d\omega'}\right|_{\omega_k} F(\omega'_{k-1}, \omega'_k, \omega_m)\,, \tag{5}$$

where

$$\begin{aligned} F(\omega'_{k-1}, \omega'_k, \omega_m) &= (\omega'_k + \omega_m)\,\ln|\omega'_k + \omega_m| - (\omega'_k - \omega_m)\,\ln|\omega'_k - \omega_m| \\ &- (\omega'_{k-1} + \omega_m)\,\ln|\omega'_{k-1} + \omega_m| + (\omega'_{k-1} - \omega_m)\,\ln|\omega'_{k-1} - \omega_m| \end{aligned}$$

and

$$\left.\frac{dA_{pq}(\omega')}{d\omega'}\right|_{\omega_k} \simeq \frac{A_{pq}(\omega'_k) - A_{pq}(\omega'_{k-1})}{\omega'_k - \omega'_{k-1}} \tag{6}$$

We also tested higher order derivative approximations, which were more complicated, but did not show a numerical advantage over this first order numerical/analytical approximation. It should be noted that the adopted

discretization automatically implies regularization, since the singularity of the integral kernel of the Hilbert transform is treated analytically. The singularities in (6) for $\omega'_k = \omega_m$ and $\omega'_{k-1} = \omega_m$ are only apparent since $\lim_{x\to 0} x \log x = 0$.

The expression (4) is satisfied by any causal function within the numerical errors due to discretization. For practical use, one needs to insure that this consistency test be verified by the line parameters within some fixed threshold ε, e.g., by checking that the residual satisfies

$$||\mathbf{b}_{pq} - \mathbf{H}\,\mathbf{a}_{pq}|| < \varepsilon$$

for each matrix entry. We tested several different norms, and we found that the maximum norm $||\cdot||_\infty = \max|\cdot|$ provides the best results since the deviations (in case of errors) are very local. Also, we found that a relative deviation within 1% insures a good causality check.

For the present application, the above consistency test must be applied to impedance and admittance f-PUL matrices. In the impedance case, it is convenient to split matrix $\mathbf{Z}(s)$ in the superposition of separate terms as

$$\mathbf{Z}(j\omega) = \mathbf{R}_0 + j\omega\mathbf{L}_\infty + \mathbf{R}_\omega(j\omega) + j\omega\mathbf{L}_\omega(j\omega) \tag{7}$$

where $\mathbf{R}_0$ is the DC part of the resistance matrix and $\mathbf{L}_\infty$ is the infinite frequency inductance matrix. Since these two terms constitute an inherently causal model, we need only to check the consistency of the frequency dependent part $\mathbf{R}_\omega(j\omega) + j\omega\mathbf{L}_\omega(j\omega)$. This separation allows to improve the numerical performance of the test. A similar procedure can be applied for the admittance representation, which can be recast as

$$\mathbf{Y}(j\omega) = j\omega\mathbf{C}_\infty + \mathbf{G}_\omega(j\omega) + j\omega\mathbf{C}_\omega(j\omega)$$

The above consistency test was applied to the four transmission line problems described in Appendix A and in [21]. These lines were verified to satisfy the above causality conditions, and are therefore consistent.

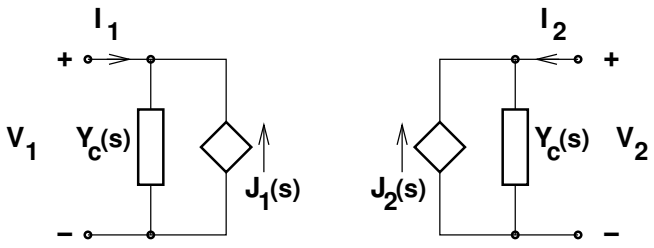

Figure 2: Basic equivalent circuit for the method of characteristics (MoC) model

3 Method of Characteristics

We give here some details on the adopted Method of Characteristics (MoC) approaches for the generation of line macromodels suitable for transient analysis. We will concentrate only on the critical aspects related to the treatment of lossy and dispersive lines with the MoC, and we will skip the basic derivation. The reader is referred to the relevant literature for further details (see, e.g., [1, 7, 11, 17, 18, 19]).

The transmission line segment is treated as a multiport, where we denote by $\mathbf{V}_1(s), \mathbf{I}_1(s)$ the input (near end) and by $\mathbf{V}_2(s), \mathbf{I}_2(s)$ the output (far end) terminal voltage-current port quantities in the Laplace (s) domain. In the MoC model, the solution of the Telegrapher's transmission line equations (1) can be reduced to the circuit equations corresponding to Fig. 2, or

$$\mathbf{I}_1(s) = \mathbf{Y}_c(s)\mathbf{V}_1(s) - \mathbf{J}_1(s), \qquad \mathbf{I}_2(s) = \mathbf{Y}_c(s)\mathbf{V}_2(s) - \mathbf{J}_2(s) \tag{8}$$

where $\mathbf{J}_1(s), \mathbf{J}_2(s)$ are currents of controlled current sources defined as

$$\mathbf{J}_1(s) = \mathbf{H}(s)\left[\mathbf{Y}_c(s)\mathbf{V}_2(s) + \mathbf{I}_2(s)\right], \qquad \mathbf{J}_2(s) = \mathbf{H}(s)\left[\mathbf{Y}_c(s)\mathbf{V}_1(s) + \mathbf{I}_1(s)\right], \tag{9}$$

with

$$\mathbf{\Gamma}^2(s) = \mathbf{Y}(s)\mathbf{Z}(s), \qquad \mathbf{Y}_c(s) = \mathbf{\Gamma}^{-1}(s)\mathbf{Y}(s), \qquad \mathbf{H}(s) = e^{-\mathcal{L}\mathbf{\Gamma}(s)} \tag{10}$$

being the squared propagation matrix, the characteristic admittance matrix, and the propagation operator, respectively. We note that the basic MoC formlation can also be cast in a Thevenin-like form. However, the adopted admittance/current source equivalent circuit is more suitable for lines with dominant metal losses with respect to

dielectric losses, since all relevant line transfer functions are bounded. Furthermore, this formulation can also be efficiently implemented in a Modified Nodal Analysis (MNA) description.

For a lossless line, the characteristic admittance matrix is constant, and the propagation operator $\mathbf{H}(s)$ reduces to a matrix of pure delays. In this case, the conversion of (8) into time domain is straightforward. In the lossy case, both characteristic admittance and propagation operator are irrational functions of the complex frequency s. Consequently, the time-domain formulation requires some form of approximation of the inverse Laplace transform. Following a common practice in linear macromodeling we will use a rational approximation in frequency domain combined with analytical inversion of the corresponding pole/residue expansion. Although this is a standard approach, special care must be taken in the specific implementation, since the accuracy and the robustness of the approximation process depends on a number of key points, which are highlighted below.

3.1 Delay extraction

The direct rational approximation of the propagation operator $\mathbf{H}(s)$ over a broad frequency band is very difficult since this matrix takes into account the line delay (henceforth the phase has fast variations) and the line attenuation/dispersion terms (characterized by slow variations in both magnitude and phase). Therefore, following the MoC approach, we extract the delay terms, which can be computed separately from the f-PUL matrices. This procedure, detailed below, insures that any excitation signal entering one end of a transmission line segment will appear at the other end only after the time-of-flight delay. This condition is often referred to as "TL-causality".

First, let us refer to a scalar line. The line delay is defined by the infinite frequency asymptotic values of capacitance and inductance as $T = \mathcal{L}\sqrt{C_\infty L_\infty}$. The propagation operator becomes in this case

$$\begin{aligned} H(s) &= \exp\left\{-\mathcal{L}\sqrt{(R_0 + sL_\infty + R_\omega(s) + sL_\omega(s))(sC_\infty + G_\omega(s) + sC_\omega(s))}\right\} \\ &= \exp\left\{-\mathcal{L}\sqrt{s^2 C_\infty L_\infty + \eta(s)}\right\} \\ &= \exp\{-sT\}\, P(s) \end{aligned} \tag{11}$$

where the dominant term at $s = \infty$ has been factored out as a pure delay term. The remaining part $P(s)$

corresponds to the delayless propagation operator and takes into account the effects due to line dispersion and attenuation. For the line cases being considered in this work, the behavior of the f-PUL parameters is such that the remainder $\eta(s) = O(s^\alpha)$ for large s, with $1 < \alpha < 2$ (in the pure skin effect case we have $\alpha = 1.5$). As a result, the delayless propagation operator $P(s) \to 0$ for $s \to \infty$. The asymptotic value at DC can also be computed easily. Since we consider a vanishing dielectric loss at DC, i.e., $G(s = 0) = 0$, we have $P(0) = 1$. In summary, the resulting transfer function $P(s)$ is bounded between 0 and 1, and has a slowly varying magnitude and phase. Therefore, its rational approximation is easy to compute.

We turn now to the multiconductor case. The set of modal delays $\{T_k\}$ are defined as

$$T_k = \mathcal{L}\,\sqrt{\Lambda_k},$$

where $\{\Lambda_k\}$ are the eigenvalues of matrix $\mathbf{C}_\infty\,\mathbf{L}_\infty$. Note that the modal delays can be quite different in case of lines embedded in a non-homogeneous dielectric. Also, we denote the matrix collecting the eigenvectors corresponding to $\{\Lambda_k\}$ as $\mathbf{M}_\infty$. More care should be taken in this case for extracting these delays, since pre-multiplication or post-multiplication of $\mathbf{H}(s)$ by pure delay terms leads to different results due to the fact that the involved matrices do not commute. The ideal solution would be to treat all modes independently, via diagonalization of $\mathbf{H}(s)$. However, in general, the modal decomposition matrices are frequency-dependent. Even in some common cases their frequency behavior is so complex that the approximation of single modes throughout the frequency axis is intrinsically ill-conditioned. We tested many different approaches, and we realized that the best strategy for extracting delays is to define the delayless propagation operator as

$$\mathbf{P}(s) = \mathrm{diag}\{e^{sT_k}\}\,\mathbf{M}_\infty^{-1}\,\mathbf{H}(s)\,\mathbf{M}_\infty. \tag{12}$$

Note that an asymptotic modal decomposition of $\mathbf{H}(s)$ is performed at $s = \infty$. This guarantees that the modal delays, which are just defined from f-PUL matrices evaluated at $s = \infty$, can be extracted via multiplication by a diagonal matrix $\mathrm{diag}\{e^{sT_k}\}$. This definition of $\mathbf{P}(s)$ corresponds to a (approximate) modal operator matrix, which is to be applied to the set of modal waves for the description of line dispersion and attenuation.

Another possible definition that was tested involves factorization of the delay terms as

$$\mathbf{P}'(s) = \exp\left\{s\mathcal{L}\sqrt{\mathbf{C}_\infty \mathbf{L}_\infty}\right\} \mathbf{H}(s) \tag{13}$$

However, this definition has the drawback that the resulting operator acts on the "conductor" quantities and not on the modal quantities. The various entries of the $\mathbf{P}'(s)$ matrix result less smooth and more difficult to approximate with rational functions. For this reason it was found that line segmentation was necessary in order to reduce line losses of a single segment and guarantee a smoother behavior. This fact has an obvious impact on the transient simulation time, since the complexity of the line macromodel is proportional to the number of line segments that are to be used.

The delay extraction is performed in (12) by pre-multiplication by a diagonal delay matrix. Similarly, a post-multiplication would lead to an almost-equivalent operator. These two alternatives are fully equivalent for lines with frequency-independent modes, like, e.g., symmetric coupled lines. This is the case for the MCM and PCB lines presented in Appendix A. However, if lines with frequency-dependent modes are treated (like, e.g., the chip interconnect), we found that an even more stable approximation can be obtained with a symmetric delay extraction, defined as

$$\mathbf{P}''(s) = \mathrm{diag}\{e^{sT_k/2}\}\, \mathbf{M}_\infty^{-1}\, \mathbf{H}(s)\, \mathbf{M}_\infty \mathrm{diag}\{e^{sT_k/2}\}. \tag{14}$$

This involves marginal overhead in the final implementation, but significantly improves the accuracy, since the off-diagonal entries of the propagation operator result smoother and easier to approximate with rational functions.

We summarize this section by noting that several choices are possible for the extraction of the line delay. The particular technique that should be adopted depends on the processing that will be applied to the delayless transfer functions. In this respect, we remark the very recent methodology that was introduced in [6]. This technique allows extraction of the delay terms via factorization of the exponential stamp of the transmission line using a modified Lie product. This elegant technique allows both delay extraction and preservation of passivity at the same time, when employed in the framework of Matrix-Rational Approximation (MRA) based macromodeling. Further comparisons and cross-validations between MRA-based and MoC-based are highly desirable and will be the subject or future investigations. These investigations should also clarify what are the advantages of the

two methodologies for particular classes of structures. For instance, delay extraction is mandatory for long or low-loss structures, but might be less critical for very short or high-loss lines. Such structures can be analyzed with very good efficiency by MRA-based techniques. A preliminary assessment has been attempted in [15] on a limited number of cases. However, significant advances on line macromodeling have been achieved in the last few months, and a more exhaustive analysis using the most recent algorithms on a large number of line cases is needed. A meanungful accuracy/efficiency analysis requires all algorithms to be implemented on the same computer platform. Steps are being taken in this direction, and will be documented in future reports.

3.2 Rational approximation

As mentioned above, the conversion into time-domain of (8)-(9) is an easy task if all transfer matrices are rational (with pure delay terms). Therefore, we approximate both characteristic admittance and delayless propagation operator as

$$\mathbf{Y}_c(s) \simeq \sum_n \frac{\mathbf{R}_n^Y}{s - p_n} + \mathbf{Y}_\infty \qquad \mathbf{P}(s) \simeq \sum_n \frac{\mathbf{R}_n^P}{s - q_n} + \mathbf{P}_\infty \tag{15}$$

We tested different strategies for the generation of this approximation. One choice was to apply the well-known technique of vector-fitting [13], which is known to produce very accurate estimates for the poles and consequently for the overall approximation. Another simple approximation algorithm was also designed, based on the determination of the location of real poles only within the band of available frequency points by means of an iterative bisection placement. This algorithm is at the basis of a macromodeling tool named TOPLine [8]. Due to the smoothness of the functions being approximated, both approximation algorithms led to very good accuracies with relatively few poles (on the order of 6-10) for all lines under investigation.

It has to be noted that these types of rational appoximations lead to excellent accuracy within the bandwidth of available frequency points. However, the behavior of the approximations outside the frequency band may lead to strange, and even to non-passive behavior. Therefore, we found to be important to have some control over the approximation throughout the complete frequency axis. This problem was solved by enforcing asymptotic constraints at both $s = 0$ and $s = \infty$ in the rational fit. This corresponds to matching the zeroth-order moments

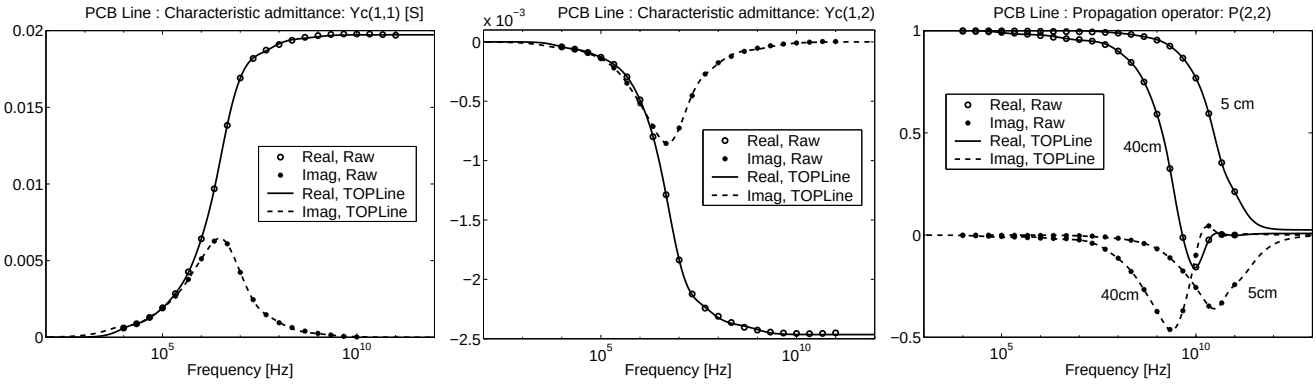

Figure 3: Rational approximation of characteristic admittance and propagation operator elements for the PCB Line case.

at these two frequency points. In particular, moment matching at $s = 0$ insures good late time behavior of the transient responses, while matching at $s = \infty$ guarantees good accuracy for short times. The latter is a quite desirable feature if the line macromodel is going to be simulated in a time-stepping transient analysis. As an example, we report in Figure 3 the rational approximation for relevant entries of $\mathbf{Y}_c(s)$ and $\mathbf{P}(s)$ for the PCB Line case.

3.3 Passivity

A few remarks about macromodel passivity. This is a critical issue, since any non-passive macromodel can hardly be used in a practical transient analysis since time instability might occur depending on the termination networks. It has to be recognized that there is no a priori guarantee of passivity for the proposed methodology. Therefore, some passivity check must be performed to detect a posteriori whether some passivity violation occurs. We remark that the excellent accuracy that is achieved by a careful delay extraction strategy combined with a good rational approximation algorithm (see, e.g., Figure 3) insures that passivity violations are small, if any. For all the cases that were investigated we experienced no passivity violations. In any case, if some violations occur by applying the proposed methodology to other transmission line cases, some passivity correction can be applied following, e.g., one of the procedures detailed in [9, 10, 14, 3, 22]. These very recent and powerful techniques allow the enforcement of passivity by insuring a minimal perturbation on the macromodel accuracy. Therefore,

even though performed via a two-step process (rational approximation and then passivity enforcement), the final macromodel may be constructed as passive, even in the MoC framework.

The passivity issue is well addressed in [4], where a completely different macromodeling strategy based on Matrix Rational Approximations (MRA) is developed. This technique provides an explicit guarantee of passivity and generates a purely lumped equivalent of the line. Unfortunately, any lumped equivalent provides only an approximation of the line delay, leading to an intrinsic violation of the TL-causality condition. Typically, the signature of such violation in the macromodel responses is the presence of early-time oscillations. Some control on these oscillations can be obtained in this framework using some "low pass" constraints in the generation of the MRA, as in [5]. In any case, some check must be performed in order to insure that the causality violation is under control (e.g., smaller than a given threshold throughout the time-of-flight of the excitation signal through the line). We could denote this as "weak TL-causality". This approach appears to be feasible for short lines, but delay extraction seems to be a key point for the analysis of long lines (e.g., the cable example of Appendix A). It is fair to say that MoC-based transmission line macromodeling provides strict TL causality with a weak enforcement of passivity, independently of the nature of the interconnect. The converse is true for MRA-based macromodeling. The generation of a strictly passive and strictly TL-causal macromodel still remains an unsolved problem and deserves further research. A promising step forward in this direction is provided by the very recent results in [6], where a new procedure for a delay extraction allowing the enforcement of a-priori passivity is devised. Further comparisons and assessments of the two complementary strategies will be documented in future reports.

3.4 Time step control

The important issue of adaptive time stepping arises when the macromodel is implemented as part of a circuit simulation environment. Actually, all modern circuit solvers have sophisticated time step control strategies for the computation of an accurate solution with a minimal number of time steps. Therefore, one possibility is to rely on the native step control algorithm (of PowerSPICE for the present work) without taking particular measures. This approach is likely to work well for circuit-based realizations, i.e., macromodels synthesized in the circuit

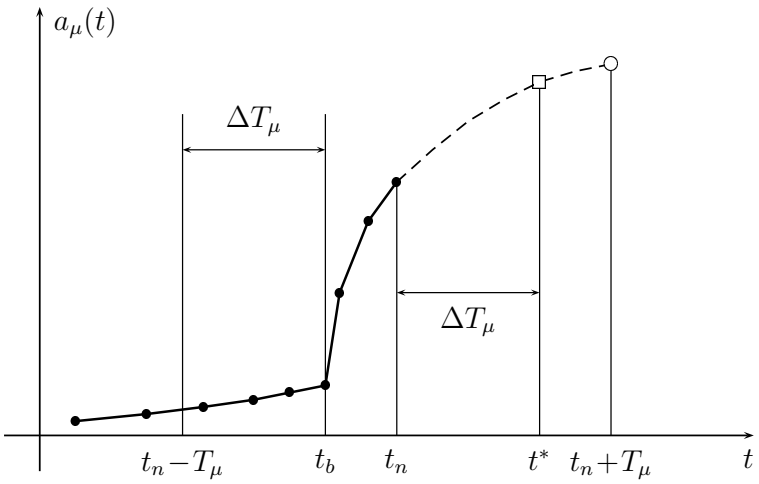

Figure 4: Schematic illustration of the time step control algorithm. See main text for details.

solver via standard circuit elements. However, for equation-based realizations based on dedicated software code responsible for the internal macromodel representation, the entire line dynamic behavior is hidden from the native step control algorithm, which in this case does not have enough information to determine the optimal time step during the transient simulation. Nonetheless, it can be shown that the accuracy of the transient simulation can be improved dramatically by adding a few simple constraints to the native time step control algorithm, as detailed below.

For illustration, consider the typical situation of a source with a piecewise linear waveform. This is also the case for the four benchmark problems considered in this work. When this source is applied to one end of the line, its waveform will be split according to the modal decomposition into the various modes. Each mode will propagate along the line with a specific delay. Henceforth, possible singularities might appear at the other line end in correspondence of each breakpoint of the input retarded by any modal delay. In addition, this occurs recursively for each line reflection in case of non-matched loads. If the time step is left unconstrained with respect to these modal delays, poor accuracy may result. For this reason, a hard constraint on the time step was added to the equation-based implementation of the proposed macromodel (to be discussed in Section 4) in order to capture any possible singularity after propagation across the line. This was possible due to a particular feature of the PowerSPICE API, which allows to set so-called ”time cusps” (i.e., times at which a time step is forced).

We refer to the situation depicted in Fig. 4, representing a snapshot of some transient waveform during the time iterations. In the plot the variable $a_\mu(t)$ denotes one of the modal current waves impinging into one of the line terminations, or, equivalently, one of the internal states for the equation-based implementation. The snapshot is taken at time t_n, so that the set of points which have already been computed in the past iterations is $\{t_k,\ k \leq n\}$. These points are represented by black dots in the figure. The purpose is to determine the location of the next time step t_{n+1}. To this end, we assume that the modal propagation delay for the considered mode is T_μ. The time values of mode a_μ that are relevant for the computation of the solution at times $t > t_n$ correspond to $t \geq t_n - T_\mu$. Therefore, the structure of the previously computed solution in the time interval $(t_n - T_\mu, t_n)$ is used for the determination of the next time step. Note that we are considering the case of a waveform singularity located at time t_b in the past, which we assume to have been well captured by the step control algorithm.

First, we need to detect whether some singularity is present in this time interval. A simple estimate of the second derivative at the previously computed points is sufficient for this purpose. As a result, each point is flagged as "singular" or "non singular". The following cases may occur

- There are no singular points in $(t_n - T_\mu, t_n)$. In such case the only constraint that is strictly necessary is $t_{n+1} \leq t_n + T_\mu$, since the MoC model requires this limitation for the validity of its defining equations. A time cusp is therefore forced at $t = t_n + T_\mu$ (circle).

- There is at least a singular point. Let t_b denote the first singular point starting from $t_n - T_\mu$ and moving forward in time. We define the corresponding time lag as $\Delta T_\mu = t_b - (t_n - T_\mu)$. The next time step will be constrained according to $t_{n+1} \leq t_n + \Delta T_\mu$. This constraint insures that the waveform to be processed at a whole for the computation of the next time iteration is smooth, and consequently the piecewise linear approximation which is implicit in the computation of the recursive convolution integrals holds with good accuracy. A time cusp is therefore forced at $t = t^* = t_n + \Delta T_\mu$ (square).

The above procedure is repeated for each mode and the resulting minimum time step is selected for next iteration. Note that the above procedure allows for both time step refining or coarsening according to the structure of the

solution being computed. Note also that the time cusps that are forced by the above procedure are additional to the further constraints that are already set by the native step control algorithm. Therefore, if the transient solution of the MNA equations of the overall network requires a smaller time step, this latter will be the one adopted for the actual iteration. The upper limit for all time steps will be the minimum modal delay time in any case.

4 Numerical Results

We report in this section transient results for the four transmission line problems described in Appendix A. Each case is solved with various line macromodels, and the results are compared in terms of accuracy and execution times.

4.1 Reference Solution

The transmission lines analyzed in this work are terminated by linear networks. Therefore, it is possible to compute a highly accurate reference solution through standard frequency-domain analysis and inverse FFT in order to recover the transient time-domain waveforms. For this analysis the termination voltages and currents have been computed vs. frequency within the band of interest. Since inverse FFT requires the time-domain waveforms to be periodic, we have periodized the excitation voltage source using a trapezoidal pulse train with the same rise/fall time and sufficient duration at the high and low levels. This duration was set longer than the time required for the transients due to line reflections to settle to their steady-state levels.

We remark that a very large number of frequency points is necessary for this type of analysis. Therefore, it has been necessary to interpolate the frequency-domain samples of the f-PUL parameter matrices in some way throughout the frequency axis in order to apply inverse FFT over a sufficient number of samples and recover transient waveforms. This interpolation could in principle violate the causality relations in the response of the system, and could produce spurious results. However, this issue arises only when the parameters are poorly

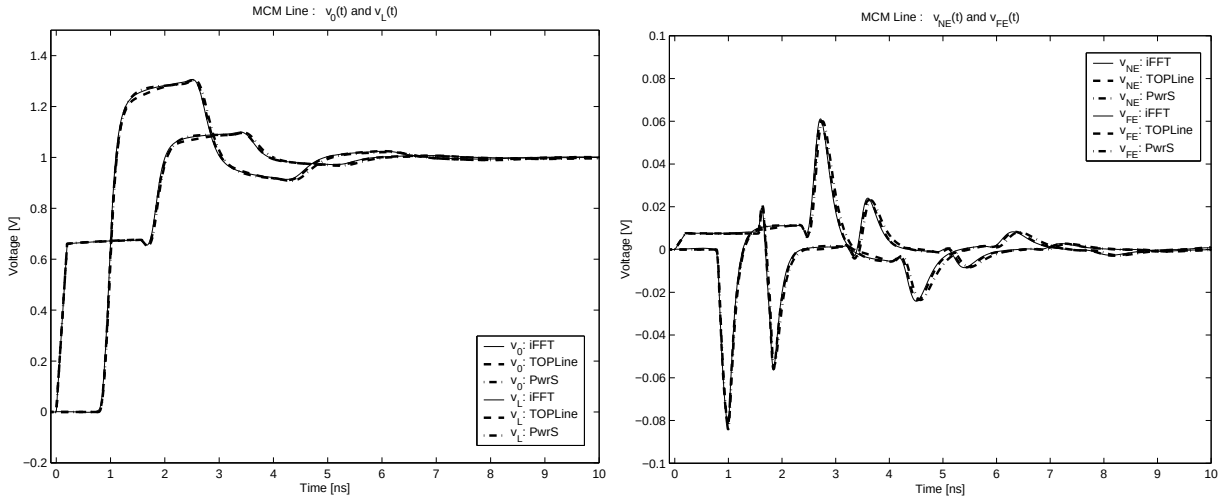

Figure 5: MCM line. Transient voltages at near and far teminations of active line (left) and victim line (right).

sampled. The presently available dataset for the specification of the lines does not appear to be critical in this respect. Therefore, the FFT-based reference curves for the three test problems will be regarded as the most accurate solutions for accuracy comparisons, and will be labeled in the plots with "iFFT".

4.2 Accuracy Analysis

We compare in this section the accuracy of two different line macromodels that were developed independently. These will be labeled as

TOPLine: this implementation is based on the application of recursive convolutions based on the rational approximation defined by (12)-(14). See also [8]. The specific computation of the rational approximation, as noted in Section 3, is performed with an ad hoc algorithm involving explicit enforcement of the zero-th order moments at DC and infinite frequency and inclusion of bandlimited real poles only.

PwrS: this implementation is also based on application of recursive convolution, but the main rational approximation process is based on Vector Fitting. The delay extraction is performed via expression (13).

The comparison between the reference solution and the results of transient simulations with the two line macromodels are depicted in Figures 5-10. The notations for waveform labeling are the same in all plots. Namely, v_0, v_L denote the near and far termination voltages of the active (driven) line, whereas v_{NE}, v_{FE} denote the near and far end crosstalk voltages. The same comments apply for all simulations: the overall accuracy that can be obtained with the two different approaches is very good. Only marginal discrepancies can be noted in some plots. However, even the sensitive waveforms of near and far end crosstalk voltages are recovered with very good accuracy.

We remark that the line macromodels that are investigated in this paper are aimed at system-level simulations for Signal Integrity assessments. In such framework, realistic models must be used not only for the transmission lines, but also for their termination networks. The latter are obviously nonlinear due to the intrinsic nature of typical drivers/receivers used in actual applications. The proposed line macromodels have been successfully applied also with nonlinear terminations. Some results are available, e.g., in [24]. In this work we concentrate on linear terminations since we need an independent solution (computed in frequency domain) to validate our macromodels with.

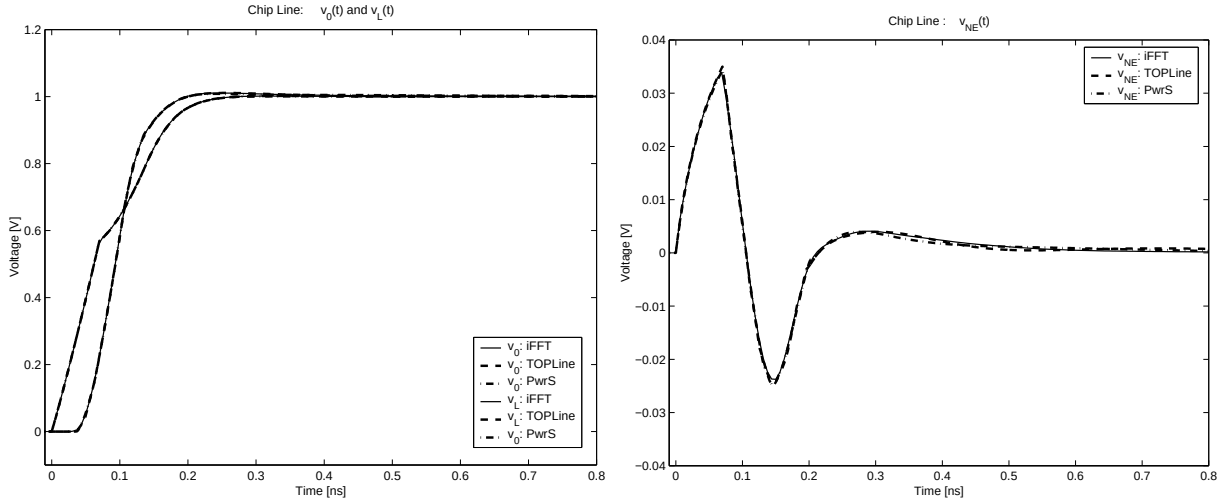

Figure 6: On-chip line. Transient voltages at near and far teminations of active line (left) and victim line (right)

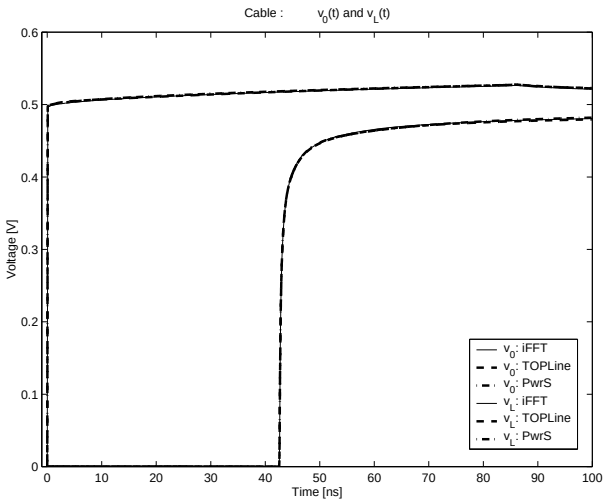

Figure 7: Cable. Transient voltages at line teminations

4.3 Timing Analysis

We present here the execution time for three different realizations of the TOPLine line macromodeling algorithm. The purpose of this section is to show that the specific strategy for the implementation of a macromodel heavily determines its numerical efficiency. For this reason, in order to guarantee a fair comparison of execution times, the three implementations that are used for this analysis are obtained here starting from the *same* delay-pole-residue approximations for each line case. Also, we remark that all simulation times reported here are obtained with a fixed time step, which is set small enough for capturing the structure of the solution with good accuracy. The three TOPLine implementations differ substantially in the practical circuit realization for the PowerSPICE solver. These differences are outlined below.

External Circuit: This implementation is the only possible without access to the kernel of the circuit solver. The macromodel is generated off-line for each line under investigation as a netlist of circuit elements corresponding to a realization of (8)-(9) combined with (15). Only standard circuit elements are used for this synthesis, in particular resistors, capacitors, controlled sources and ideal delay lines (the latter to synthesize the modal delays). Since this procedure is quite standard, we do not give additional details here. The reader is referred, e.g., to [2].

Internal Circuit: The adopted circuit simulation environment has the nice feature of a complete Application Program Interface (API) that enables the user to define a new device by means of dedicated C-code sub-routines, which can be compiled and linked to the main simulation engine. Therefore, the same equivalent circuit above can be implemented with both topology and element values of the macromodel equivalent circuit defined on-line during the transient simulation. This implementation is equivalent to previous one, differing only in the way the macromodel circuit elements are stamped in the MNA matrix of the overall network.

Equation-based: Due to the availability of the API for the definition of the line macromodel, it was possible to skip the equivalent circuit synthesis and to derive an equation-based implementation of (8)-(9)-(15). The circuit elements of previous implementations are replaced by properly defined internal states, which are automatically initialized, computed and stored during the transient simulation. These states correspond to the modal current waves impinging into the line terminations. The application of delayless rational functions to these states is realized through recursive convolutions (see, e.g., [2, 23]). The retardation due to propagation delays is simply obtained by keeping track of the past history of all states for a time lag larger than the maximum modal delay. The retarded modal current waves are readily available in memory

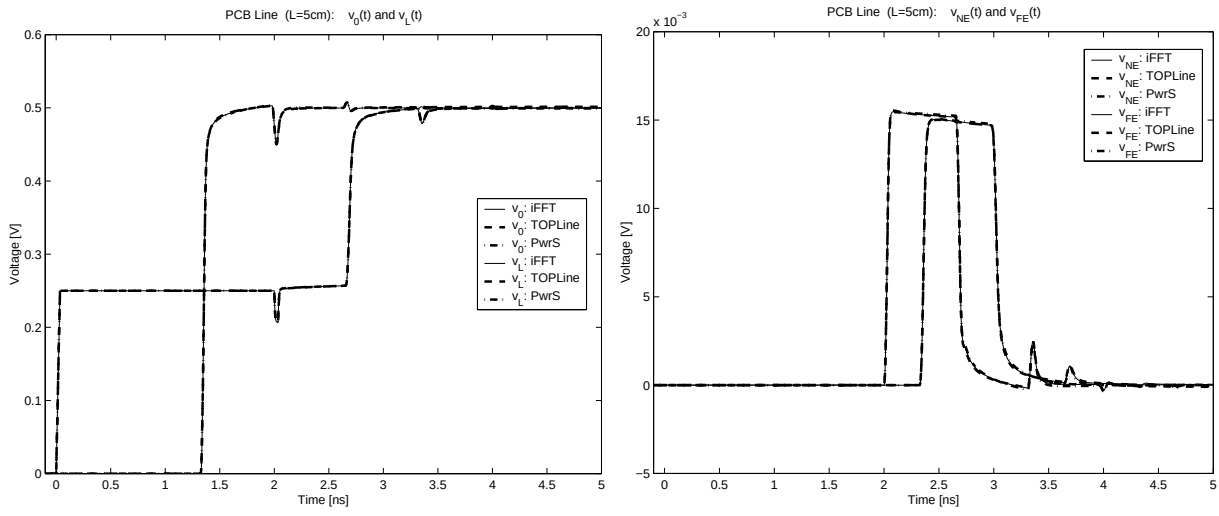

Figure 8: PCB line (5 cm). Transient voltages at near and far teminations of active line (left) and victim line (right).

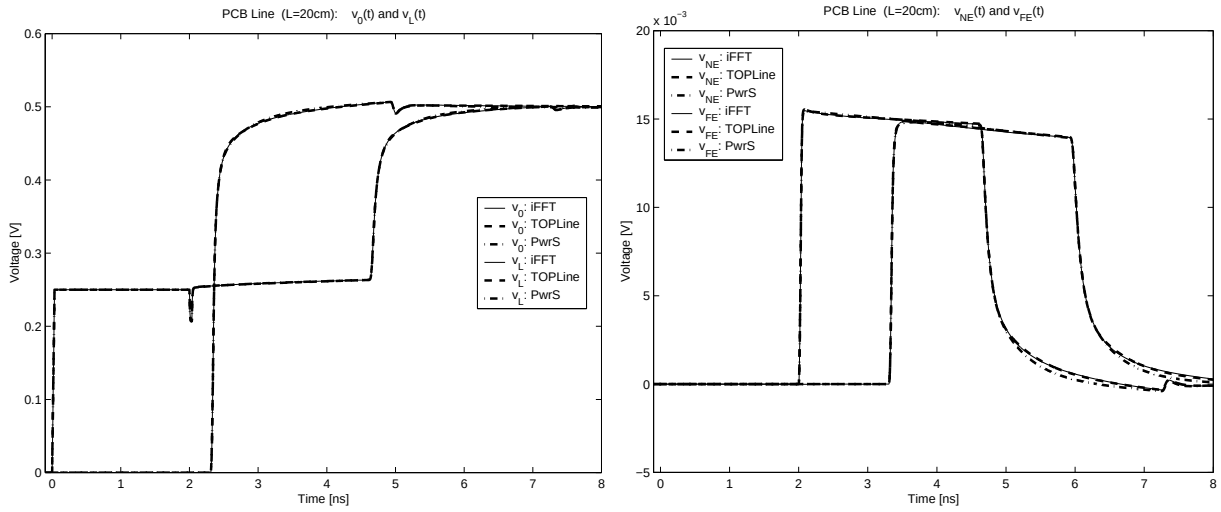

Figure 9: PCB line (20 cm). Transient voltages at near and far teminations of active line (left) and victim line (right).

for processing.

The timing result are reported in Table 1. The computer platform that was used is a Pentium IV PC (1.8 GHz) running Linux. As a general comment, we see that a significant speedup is obtained using the most efficient implementations. This is true for all cases that were analyzed and tested.

5 Conclusions

We presented in this paper several implementations of lossy transmission lines macromodels, all based on some generalized version of the well-known Method of Characteristics. The various algorithms were applied to four line examples (a chip, a module, a board, and a cable), which can be considered as a quite realistic set of benchmarks for interconnects in today's technology. All the line problems are characterized by both metal and dielectric losses, and are specified by tabulated frequency-dependent per-unit-length parameter matrices. To insure self-consistency of this dataset, a Hilbert transform-based causality check was derived and applied.

The various line macromodels analyzed in this paper share as a common background the extraction of the line

(modal) delays and the rational approximation of suitable delayless transfer functions. Several possible choices are described and discussed. Various different implementations have been produced, based on either equivalent circuit synthesis or equation-based synthesis. The latter are realized using recursive convolutions. The results show that quite good accuracies can be obtained for all line cases, even following different approximation strategies. However, the numerical efficiency in terms of execution time is heavily dependent on the particular implementation.

6 Acknowledgments

The examples provided in this paper evolved from extensive work in the transmission line modeling areas from several IBM divisions. While it is impossible to mention all contributors, we would like to acknowledge Z. Chen, A. Deutsch, R. Gravrok, A. Haridass, A. Huber, E. Klink, G. Kopcsay, and T. Winkel.

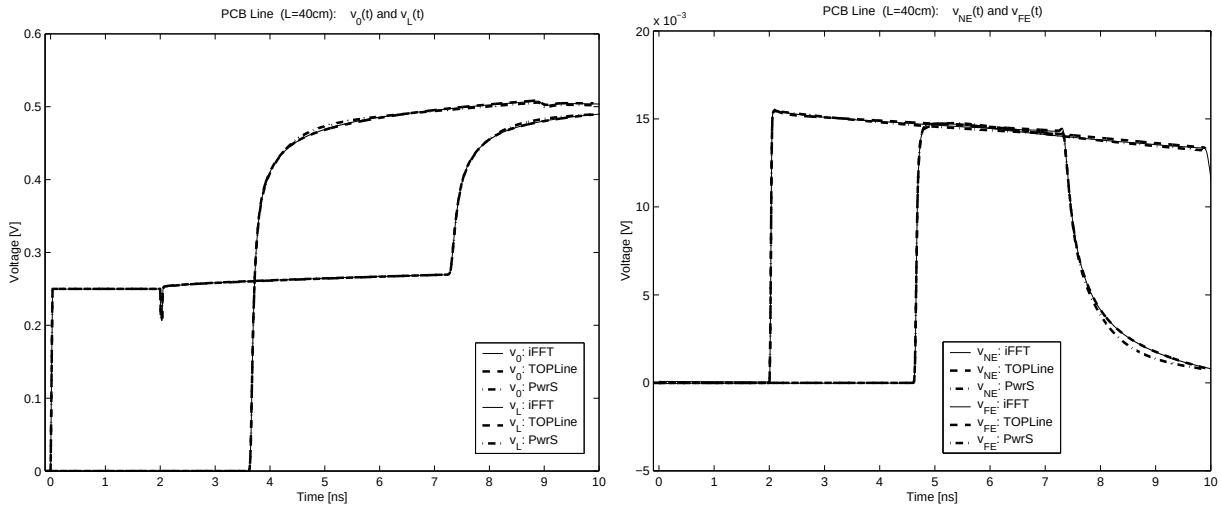

Figure 10: PCB line (40 cm). Transient voltages at near and far teminations of active line (left) and victim line (right).

Line	External Circuit	Internal Circuit	TOPLine
MCM	6.0	3.43	0.34
Chip	3.2	5.33	0.35
Cable	9.9	4.70	0.88
PCB (5cm)	13.9	10.3	2.68
PCB (20cm)	12.9	9.51	2.81
PCB (40cm)	15.4	9.12	2.64

Table 1: Execution time in seconds for all line problems.

A Four Test Problems

This section presents the four benchmark transmission line problems that are considered in this work. The four cases refer to a MCM coupled line, an on-chip coupled line, a cable, and a PCB coupled line. Therefore, these examples are quite representative of the actual situations that are typically encountered in analysis and design of high-speed digital systems. Note that this dataset is an extended version of the transmission line problems that can be found in [21]. Unless specified, all the line elements are given in normalized units, namely capacitances are in pF, resistances in kΩ, inductances in μH, frequency in GHz, time in ns, and length in cm.

MCM line

This example consists of a 10 cm long MCM coupled line. The two line conductors are terminated by 30 Ω resistors at the near end and by two 1.5 pF capacitors on the far end. The input signal is a saturated ramp with rise time $t_r = 0.2$ ns applied at the near end to one of the two conductors, and the required duration for transient analysis 10 ns. The four matrices of line parameters are frequency-dependent, therefore including the effects of metal (skin effect) and dielectric losses. The precise definition of the frequency-dependent parameter tables is detailed in [21], where this structure is denoted as *Line 2*. Note that the specification of the line parameters in [21] is missing an asymptotic value at very high (infinite) frequency, which is necessary for a correct definition

of the line delays and for the computation of the asymptotic values of the characteristic admittance matrix entries. Appropriate values are defined here for a frequency $f_H = 10^{50}$ GHz,

$$\mathbf{R}_H = \begin{bmatrix} 1.1268 \times 10^{22} & 7.8839 \times 10^{20} \\ 7.8839 \times 10^{20} & 1.1268 \times 10^{22} \end{bmatrix} \mathrm{k\Omega/cm},$$

$$\mathbf{L}_H = \begin{bmatrix} 4.5450 \times 10^{-3} & 2.4270 \times 10^{-4} \\ 2.4270 \times 10^{-4} & 4.5450 \times 10^{-3} \end{bmatrix} \mu\mathrm{H/cm}.$$

On-chip line

This example consists of a 5 mm long on-chip coupled line. The terminations are similar to the MCM coupled line above, but with different load resistance and capacitance values. Namely, $R_S = 50\,\Omega$ and $C_L = 2$ fF. The input signal is a saturated ramp with rise time $t_r = 0.07$ ns, and the required duration for transient analysis 0.8 ns. The per-unit-length capacitance matrix is constant,

$$\mathbf{C} = \begin{bmatrix} 1.79926 & -0.06759 \\ -0.06759 & 2.14866 \end{bmatrix} \mathrm{pF/cm}$$

and there are no dielectric losses (**G**=0). The models for frequency-dependent resistance $\mathbf{R}(f)$ and inductance $\mathbf{L}(f)$ are given in Table 2.

Cable

This line is a long 10 m cable connected with 50 Ω source and load resistors. The input signal is a voltage series source launching a saturated ramp with rise time $t_r = 0.1$ ns, and the required duration for transient analysis is 100 ns. The per-unit-length parameters are defined in [21], where the structure is denoted as *Line 4*. As for the MCM line above, the high-frequency point is introduced at $f_H = 10^{50}$ GHz. The corresponding values are

$$R_H = 8.8423993 \times 10^{20}\,\mathrm{k\Omega/cm}\,, \qquad L_H = 2.104140 \times 10^{-3}\,\mu\mathrm{H/cm}.$$

Freq.	R_{11}	R_{12}	R_{22}	L_{11}	L_{12}	L_{22}
0.0000	54.980e-3	0.0	333.700e-3	14.024e-3	11.186e-3	14.1697e-3
0.0010	56.440e-3	1.4094e-3	335.550e-3	14.024e-3	11.186e-3	14.1697e-3
0.0033	56.442e-3	1.4130e-3	335.555e-3	14.023e-3	11.186e-3	14.1697e-3
0.0066	56.447e-3	1.4220e-3	335.556e-3	14.020e-3	11.178e-3	14.1607e-3
0.0100	56.460e-3	1.4320e-3	335.570e-3	14.000e-3	11.167e-3	14.1530e-3
0.0330	56.677e-3	1.4408e-3	335.785e-3	13.840e-3	11.012e-3	14.0030e-3
0.0660	57.326e-3	2.0620e-3	336.430e-3	13.365e-3	10.557e-3	13.5740e-3
0.1000	58.260e-3	2.9540e-3	337.360e-3	12.710e-3	9.9300e-3	12.9820e-3
0.3000	63.800e-3	8.2570e-3	342.875e-3	9.3000e-3	6.6760e-3	9.90400e-3
0.6600	68.337e-3	12.560e-3	347.375e-3	7.1279e-3	4.6030e-3	7.94560e-3
1.0000	70.375e-3	14.454e-3	349.380e-3	6.5050e-3	4.0090e-3	7.38400e-3
3.5000	77.443e-3	20.320e-3	356.416e-3	5.6750e-3	3.2260e-3	6.64500e-3
6.6000	84.188e-3	24.549e-3	363.250e-3	5.5130e-3	3.0874e-3	6.49600e-3
10.0000	92.682e-3	29.190e-3	371.725e-3	5.4160e-3	3.0180e-3	6.40900e-3
1E50	891.77e-3	992.50E-3	9999.17e-3	4.8606e-3	2.7798e-3	5.68600e-3

Table 2: Frequency-dependent resistance and inductance matrix entries for the on-chip line. Units are GHz for frequency, kΩ/cm for resistance, and μH/cm for inductance.

PCB coupled line

This example is a lossy board coupled line with more complex loading networks including three lossless (ideal) lines as specified in [21]. This termination scheme is a simplified model of a typical TDR/TDT measurement setup, including a few lumped shunt capacitances for discontinuities modeling. All the line parameters are listed at selected frequency points in [21], where this structure is denoted as *Line 6*. The length $\mathcal{L}$ of the lossy coupled line section can be either 5, 20 or 40 cm. The input signal is again a saturated ramp with rise time $t_r = 0.035$ ns, and the required transient analysis duration is 4 ns, 5 ns and 8 ns, respectively. Also in this case we complete the f-PUL tables with an asymptotic high-frequency point at $f_H = 10^{50}$ GHz,

$$\mathbf{R}_H = \begin{bmatrix} 7.6153 \times 10^{21} & 4.4942 \times 10^{20} \\ 4.4942 \times 10^{20} & 7.6153 \times 10^{21} \end{bmatrix} \mathrm{k\Omega/cm},$$

$$\mathbf{L}_H = \begin{bmatrix} 3.3483 \times 10^{-3} & 4.1833 \times 10^{-4} \\ 4.1833 \times 10^{-4} & 3.3483 \times 10^{-3} \end{bmatrix} \mu\mathrm{H/cm},$$

$$\mathbf{C}_H = \begin{bmatrix} 1.282800 & -0.160270 \\ -0.160270 & 1.282800 \end{bmatrix} \mathrm{pF/cm},$$

$$\mathbf{G}_H = \begin{bmatrix} 7.576450 & -0.9465830 \\ -0.9465830 & 7.576450 \end{bmatrix} \mathrm{mS/cm}.$$

References

[1] F. H. Branin, "Transient Analysis of Lossless Transmission Lines", *Proc. IEEE*, Vol. 55, 1967, pp. 2012–2013.

[2] M. Celik, L. Pileggi, A. Obadasioglu, *IC Interconnect Analysis*, Kluwer, 2002.

[3] H. Chen, J. Fang, "Enforcing Bounded Realness of S Parameter Through Trace Parameterization", in *Digest of Electr. Perf. Electronic Packaging*, Vol. 12, Princeton, NJ, October 2003, pp. 291–294.

[4] A. Dounavis, R. Achar, M. Nakhla, “A general class of passive macromodels for lossy multiconductor transmission lines ”, *IEEE Trans. MTT*, Vol. 49, 2001, 1686–1696.

[5] A. Dounavis, R. Achar, M. Nakhla, “Addressing transient errors in passive macromodels of distributed transmission-line networks”, *IEEE Trans. MTT*, Vol. 50, 2002, 2759–2768.

[6] A. Dounavis, N. Nakhla, R. Achar, M. Nakhla, “Delay Extraction and Passive Macromodeling of Lossy Coupled Transmission Lines”, in *Digest of Electr. Perf. Electronic Packaging*, Vol. 12, Princeton, NJ, October 2003, pp. 251–254.

[7] C. Gordon, T. Blazeck, R. Mittra, “Time-domain simulation of multiconductor transmission lines with frequency-dependent losses”, *IEEE Trans. Comp. Aided Design*, Vol. 11, 1992, pp. 1372–1387.

[8] S. Grivet-Talocia, F. G. Canavero, “TOPLline: a delay-pole-residue method for the simulation of lossy and dispersive interconnects”, in *Digest of Electr. Perf. Electronic Packaging*, Vol. 11, Monterey, CA, October 2002, pp. 359–362.

[9] S. Grivet-Talocia, ”Enforcing Passivity of Macromodels via Spectral Perturbation of Hamiltonian Matrices” , *7th IEEE Workshop on Signal Propagation on Interconnects (SPI), Siena (Italy)*, pp. 33-36, May 11-14, 2003

[10] S. Grivet-Talocia, ”Passivity enforcement via perturbation of Hamiltonian matrices”, submitted to *IEEE Trans. CAS-I*, 2003.

[11] A. J. Gruodis, C. S. Chang, “Coupled lossy transmission line characterization and simulation”, *IBM Journal of Research and Development*, Vol. 25, 1981, pp. 25–41.

[12] E. A. Guillemin, *Theory of linear physical systems*, John Wiley and Sons, 1963.

[13] B. Gustavsen, A. Semlyen, “Rational approximation of frequency domain responses by vector fitting”, *IEEE Trans. Power Delivery*, Vol. 14, 1999, pp. 1052–1061.

[14] B. Gustavsen, A. Semlyen, “Enforcing passivity for admittance matrices approximated by rational functions”, *IEEE Trans. Power Systems*, Vol. 16, 2001, 97–104.

[15] I. M. Elfadel, A. Dounavis, H.-M. Huang, M. S. Nakhla, A. E. Ruehli, R. Achar, “Accuracy and Performance of Passive Transmission Line Macromodels Based on Optimal Matrix Rational Approximations”, in *Digest of Electr. Perf. Electronic Packaging*, Vol. 11, Monterey, CA, October 2002, pp. 351–354.

[16] J. D. Jackson, *Classical Electrodynamics, 2nd Ed.*, New York: Wiley, 1975.

[17] D. B. Kuznetsov, J. E. Schutt-Aine, “Optimal transient simulation of transmission lines”, *IEEE Transactions on Circuits and Systems–I*, Vol. 43, 1996, pp. 110–121.

[18] S. Lin, E. S. Kuh, “Transient simulation of lossy interconnects based on recursive convolution formulation”, *IEEE Transactions on Circuits and Systems–I*, Vol. 39, 1992, pp. 879–892.

[19] T. V. Ngyuen, “Transient analysis of lossy transmission lines using rational function approximations”, in *Digest of Electr. Perf. Electronic Packaging*, Vol. 2, 20–22 October, 1993, pp. 172–174.

[20] S. Ramo, J. R. Whinnery, T. Van Duzer, *Fields and Waves in Communication Electronics*, John Wiley & Sons, 1984.

[21] A. E. Ruehli, A. C. Cangellaris, H.-M. Huang, “Three test problems for the comparison of lossy transmission line algorithms”, in *Digest of Electr. Perf. Electronic Packaging*, Vol. 11, Monterey, CA, October 2002, pp. 347–350.

[22] D. Saraswat, R. Achar, M. Nakhla, “Enforcing Passivity for Rational Function Based Macromodels of Tabulated Data”, in *Digest of Electr. Perf. Electronic Packaging*, Vol. 12, Princeton, NJ, October 2003, pp. 295–298.

[23] A. Semlyen, A. Dabuleanu, “Fast and accurate switching transient calculations on transmission lines with ground using recursive convolution”, *IEEE Transactions on Power Apparatus and Systems*, Vol. 94, 1975, pp. 561–571.

[24] I. S. Stievano, Z. Chen, D. Becker, F. G. Canavero, S. Grivet-Talocia, G. Katopis, and I. A. Maio, “Modeling of on-board and on-chip interconnected digital devices,” in *2002 International Symposium on Electromagnetic Compatibility, Sorrento, Italy*, pp. 27–32, September 9–13, 2002.